Supplemental Discussion for Storage Thresholds for Relative Sea Level Signals in the Stratigraphic Record by Li, Yu, and Straub

Additional Morphodynamic and Stratigraphic Analysis

In addition to the experiments discussed in the report body, two additional experiments were performed which were characterized by 1) $H^* = 1$, $T^* = 0.5$ and 2) $H^* = 4$, $T^* = 2$. Similar to the previously discussed experiments, these experiments shared the same input water and sediment feed rates and long term sea level rise rate. In each experiment, statistically significant peaks in spectral density were found at the time scale of imposed periodicity, indicating RSL signal storage (Fig. S1). Analogous to modulated turbulence [1] and shredding of sediment flux signals [2], our results suggest that the threshold for signal shredding exists somewhere between 0.5 – 1.0 for both H^* and T^*.

Additional test were performed to search for the signature of RSL cycles in the stratigraphy and morphodynamics of experimental data sets. First, we perform an analysis of mean deposition rate time series for all experiments along a distal circular transect located at 1.1 m from the sediment and water source (Fig. S2). This location approximates the mean spatial location of the shoreline in all experiments. Similar to our analysis of stratigraphic time series at 0.6 m from the source, we start by characterizing the power spectra of our control experiment. All power spectra in this study are generated with a MultiTaper Method (MTM)[3]. We produce confidence bands for the identification of statistically significant frequencies by performing a Chi-square test on the power spectra of our control experiment with a red-noise model. For all confidence tests in this study, we assume an underlying autoregressive-1 “red noise” model, as in other studies which document correlation in morphodynamic[2] and stratigraphic[4] time series. These confidence bands are then used in analysis of the experiments with imposed RSL cycles. Similar to our analysis of the proximal transect, we find that statistically significant peaks are present at the periodicity of imposed RSL cycles in experiments with H^* and/or T^* values equal to or much greater than 1. However, no peak is observed in the experiment where H^* and T^* were much less than 1. Additionally, we find that the signal strength of all peaks is reduced along the distal, relative to proximal transect, suggesting optimal signal storage likely does not occur at the mean shoreline location.

To further search for the signature of the imposed RSL cycles in the preserved stratigraphy, we generate time series of the second moment of deposition rates measured along the two transects previously discussed. Specifically, we measure the standard deviation of deposition rates calculated for each pair of sequential time lines within the stratigraphy. This is similar in spirit, but not identical to, the regional stratigraphic variability time series analysis performed by Karaitopoulos et al. in 2014[5]. Similar to our time series analysis of mean deposition rates, we find significant peaks in spectra at the imposed RSL periodicity for experiments where T^* and/or H^* were greater than 1, while no statistically significant peak is observed in the spectra of the experiment where both T^* and H^* were less than 1. Results from the proximal transect are shown in figure S3.

Next, we compare aspects of the physical and synthetic stratigraphy of the four experiments. First, we compare the fraction of colored sand preserved in strike oriented cross-sections located 0.89 m from the basin inlet point (Fig. S4A-E). The colored sand serves as a proxy for the coarse sand fraction input to the basin, as noted above. For each cross-section we calculated the fraction of the deposit composed of colored sand. Using a threshold color value, determined from visual inspection, we separated coarse colored sand deposits from fine white silica deposits. We implemented this technique using a range of plausible threshold values to assess error in our calculation. We find similar colored sand fractions preserved in the control and low H^* low T^* deposits, while the high T^* and high H^* deposits have significantly more preserved colored sand (Fig. S4F). We also compared the dimensions of preserved channel bodies in the four experiments. Channel body widths and depths were measured along the same strike transect used for our proximal stratigraphic time series analysis. From this database we calculated 25%, 50%, and 75% channel body depths and width-to-depth ratios (Fig. S4G-H). We observe significant differences in the channel body dimensions of our high H^* experiments from our control experiment, while the channel body dimensions of our two lower magnitude experiments are similar to our control experiment.

Expanded Methods

The experiments performed in this study were conducted in the Delta Basin at Tulane University's Sediment Dynamics Laboratory. This basin is 2.8m wide by 4.2m long and 0.65m deep. Accommodation is created in the Delta Basin by slowly increasing base level using a motorized weir that is in hydraulic communication with the basin. This system allows base-level control through a computer interface with submillimeter-scale resolution. Water and sediment supply to the basin are also controlled through the above-mentioned computer interface.

All experiments included an initial build out phase in which sediment and water were mixed in a funnel and fed from a single point source at the center of the upstream wall. After a system prograded ~1.1 m from the source to shoreline, the long term base-level rise was initiated at a rate equal to the total sediment discharge divided by the desired delta-top area. In each experiment, the combination of sediment feed rate and long term base-level rise allowed the shoreline to be maintained at an approximately constant location through the course of the experiment, with superimposed fluctuations associated with the imposed RSL cycles. Resulting deltas had topset slopes of ~$2x10^{-2}$ and foreset slops of ~$6x10^{-1}$ (Fig. S5).

The experiments discussed in this manuscript are as follows:

TDB-12: Following progradation with no base level rise, the control experiment was run for 1285 hrs, the final 900 hrs with constant feeds of water and sediment.

TDB-14-1: Following progradation, this experiment aggraded for 140 hrs with no RSL cycles followed by 490 hrs of base level cycling defined by cycles with $R_{RSL} = 4H_c$ and $T_{RSL} = 2T_c$.

TDB-14-2: Following progradation, this experiment aggraded for 140 hrs with no RSL cycles followed by 490 hrs of base level cycling defined by cycles with $R_{RSL} = 1H_c$ and $T_{RSL} = 0.5T_c$. This was then followed by aggradation for 50 hrs with no RSL cycles followed by 490 hrs of base level cycling defined by cycles with $R_{RSL} = 0.5H_c$ and $T_{RSL} = 0.5T_c$.

TDB-15-1: Following progradation, this experiment aggraded for 50 hrs with no RSL cycles followed by 490 hrs of base level cycling defined by cycles with $R_{RSL} = 0.5H_c$ and $T_{RSL} = 2T_c$. This was then followed by aggradation for 140 hrs with no RSL cycles followed by 490 hrs of base level cycling defined by cycles with $R_{RSL} = 2H_c$ and $T_{RSL} = 0.5T_c$.

The input sediment mixture was designed to mimic earlier experimental work[6] and had a broad distribution, ranging from 1 – 1000 μm with a mean of 67 μm, and included a small amount of a polymer to enhance sediment cohesion. A fraction of the coarse tail of the distribution was replaced with dyed sediment of near equivalent grain size to aid visualization of stratigraphic architecture. In order to aid characterization of morphodynamics the input water was dyed with a food coloring.

Three types of data were collected from the experiments: system morphology, surface topography, and deposit stratigraphy. The morphologies of the fluvial systems were recorded with a digital camera positioned to collect images of the entire delta, which were used to characterize surface dynamics once every 15 min. Topography was monitored with a FARO Focus3D-S 120 laser scanner with a 5 mm horizontal grid in the down and cross basin directions, respectively. The vertical resolution of the scanner is less than 1 mm. Topographic scans were collected once an hour for the duration of each experiment. This scanner also houses a digital camera, such that all topographic points are tagged with RGB color values, thus producing 3D photos. Each experimental stage produced an average of 120 mm of stratigraphy. Following each experiment, we sectioned and imaged the deposits along strike oriented transects 0.89 and 1.30 m from the basin infeed location.

Experimental Parameters

H_c and T_c were defined through topographic analysis of the control experiment and were then used to define the magnitude and periodicity of RSL cycles in remaining three experiments (Table S1).

Delta H_c & T_c database

Here we compile a data set of H_c and T_c estimates for field-scale basins using published data on river depths and long-term sedimentation rates, which includes 13 modern delta systems (Table S2 and Fig. S6). Our data set only utilizes sedimentation rates measured for time intervals in excess of 100 kyrs. As shown by Sadler [7], for a wide range of time scales, sedimentation rate is a function of the interval of measurement. However, Jerolmack and Sadler [8] showed that persistence in deposition rates as a function of measurement interval is reached at time scales in excess of 100 kyr for deltas.

Experiment	H_c [mm]	T_c [hr]
Control	12.5	49

	R_{RSL}	T_{RSL}
0.5 H_c 0.5 T_c	6.25	24.5
0.5 H_c 2 T_c	6.25	98
2 H_c 0.5 T_c	25	24.5
1 H_c 0.5 T_c	12.5	24.5
4 H_c 2 T_c	50	98

Table S1: Autogenic limits and RSL attributes for physical experiments.

System	*Hc* [m]	$\bar{r}$ [mm/yr]	*Tc* [kyr]
1) Orinoco - eastern Venezuela	100 [9]	2.7 [20]	371
2) Ganges - India	60 [10]	0.31 [21]	194
3) Mississippi - Southern USA	50 [11]	0.25 [22]	200
4) Yangtze - Eastern China	25 [12]	0.09 [23]	278
5) Nile - Northern Egypt	25 [13]	0.39 [24]	64
6) Yellow - Eastern China	20 [12]	0.6 [25]	33
7) Niger - Nigeria	20 [14]	0.71 [26]	28
8) Po - Northern Italy	17 [12]	1 [27]	17
9) Indus - Pakistan	15 [15]	0.07 [28]	214
10) Baram - Malaysia	12 [16]	0.43 [29]	28
11) Mackenzie - Northwest Canada	9 [17]	0.12 [30]	75
12) Rhine - The Netherlands	7 [18]	1.2 [31]	6
13) Rio Grande - Southwestern USA	5 [19]	0.71 [19]	7

Table S2: Compilation of parameters controlling autogenic space and time scales for field scale systems.

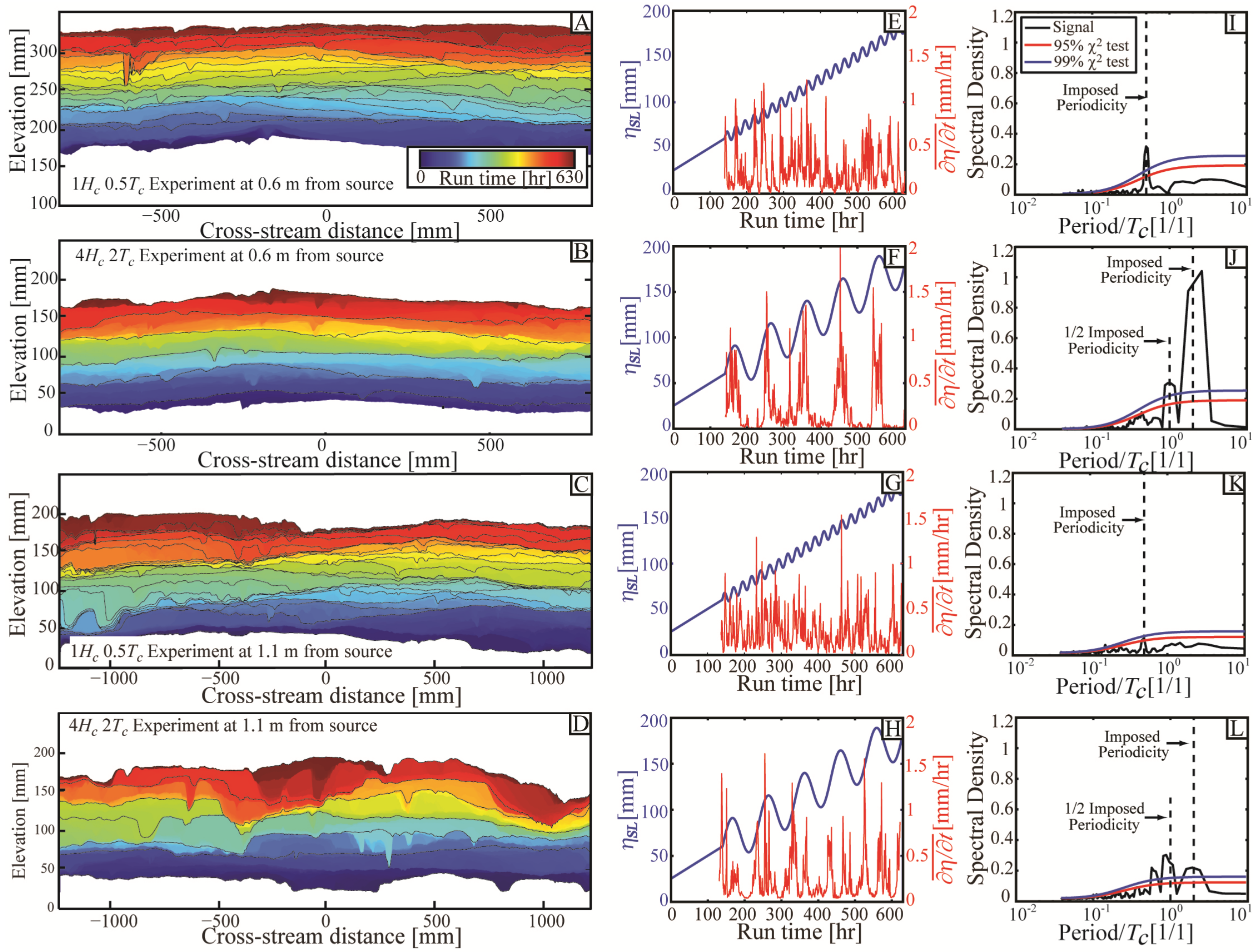

Fig. S1: **Time series analysis of mean deposition rate calculated from preserved stratigraphy for additional experiments not discussed in main report text with comparison to sea level time series.** A-D) Synthetic stratigraphy along proximal (0.6 m radius from source) and distal (1.1 m radius from source) transects. Solid black lines represent time horizons separated by 1 T_c (A) or demarcating the start of each RSL cycle (B-D). E-H) Sea level and mean deposition rate time series along distal transects; I-L) Power spectra of mean deposition rate time series and χ^2 confidence limits.

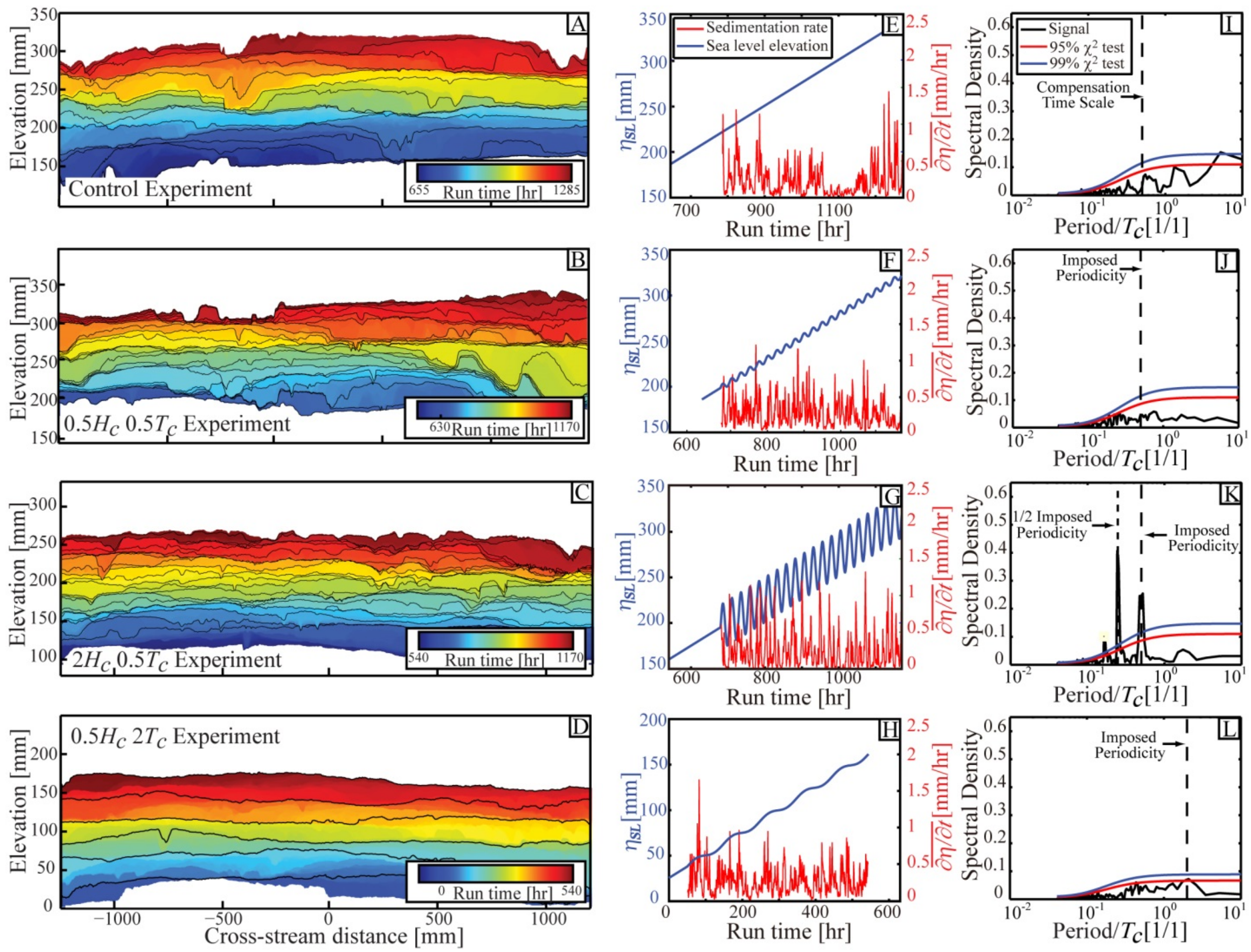

Fig. S2: **Time series analysis of mean deposition rate calculated from preserved distal stratigraphy for all experimental deltas with comparison to sea level time series.** A-D) Synthetic stratigraphy along a distal transect defined by a 1.1 m radius from source. Solid black lines represent time horizons separated by 1 T_c (A) or demarcating the start of each RSL cycle (B-D). E-H) Sea level and mean deposition rate time series along distal transects; I-L) Power spectra of mean deposition rate time series and χ^2 confidence limits.

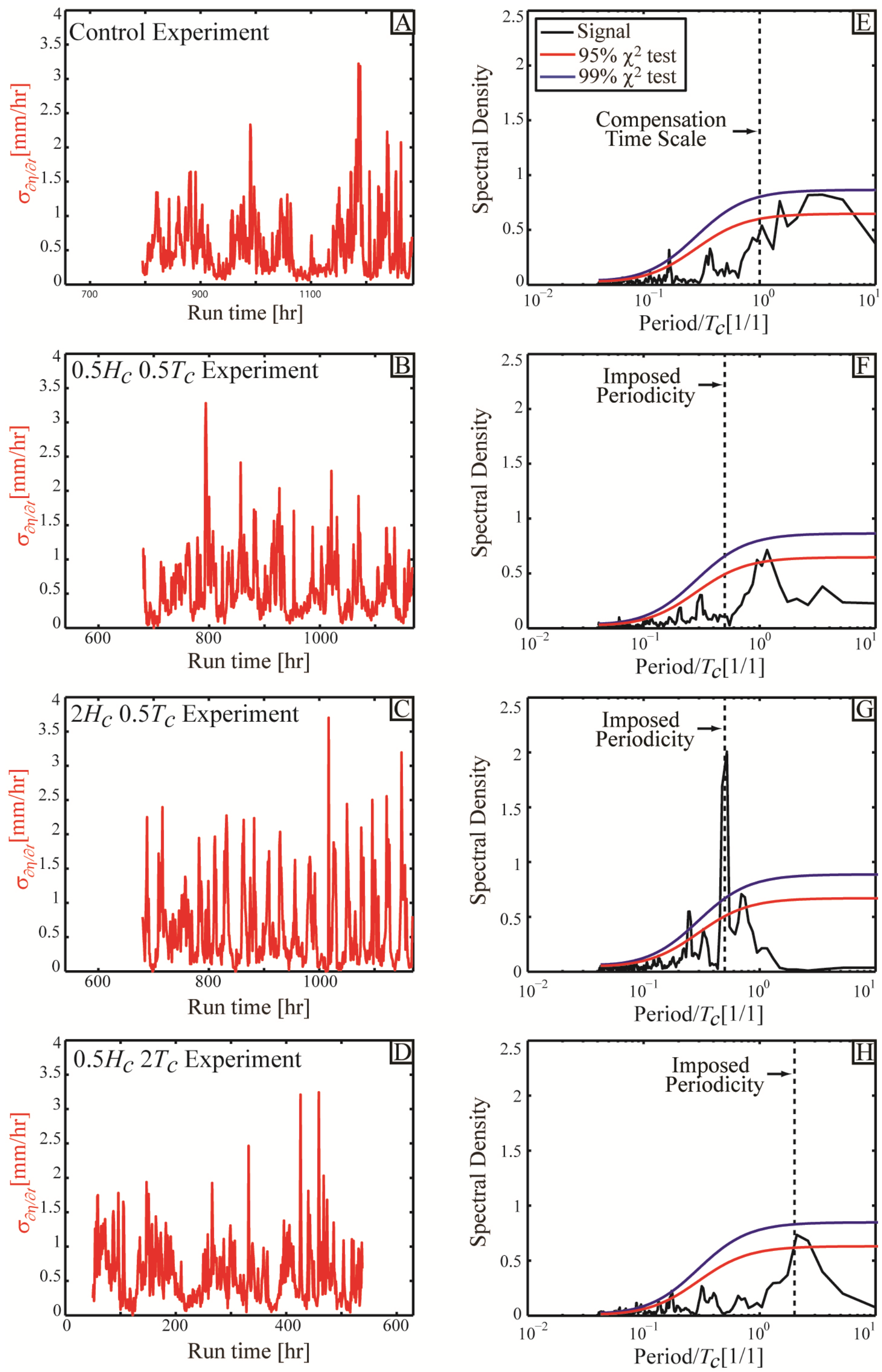

Fig. S3: **Time series analysis of the standard deviation of deposition rate calculated from preserved proximal stratigraphy for all experimental deltas.** A-D) Standard deviation of deposition rate time series along proximal transects; I-L) Power spectra of mean deposition rate time series and χ^2 confidence limits.

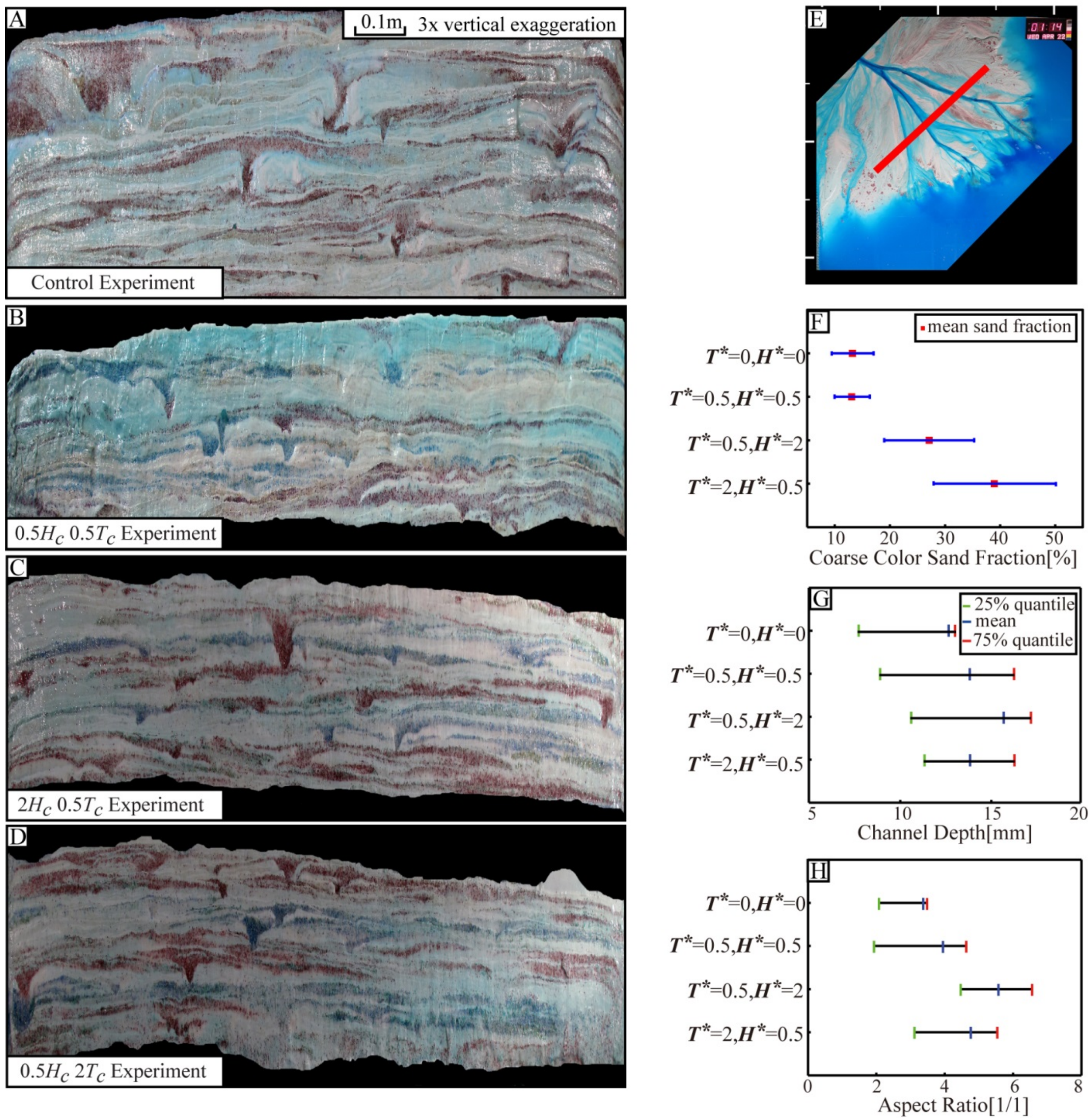

Fig. S4: **Comparison of physical stratigraphy in four experiments.** A-D) Images of physical stratigraphy displayed as if looking from source to sink. E) Overhead image of active experiment with location of stratigraphic panels shown with solid red line. F) Comparison of coarse color sand fraction in physical stratigraphic panels from each experiment. Error bars represent range of coarse colored sand fraction estimated from the range of threshold color values used to separate colored sand deposits from fine white deposits. G) Comparison of mean and range of channel depths, where range is expressed by the 1st and 3rd quartile. H) Comparison of mean and range of channel width-to-depth ratio in experiments.

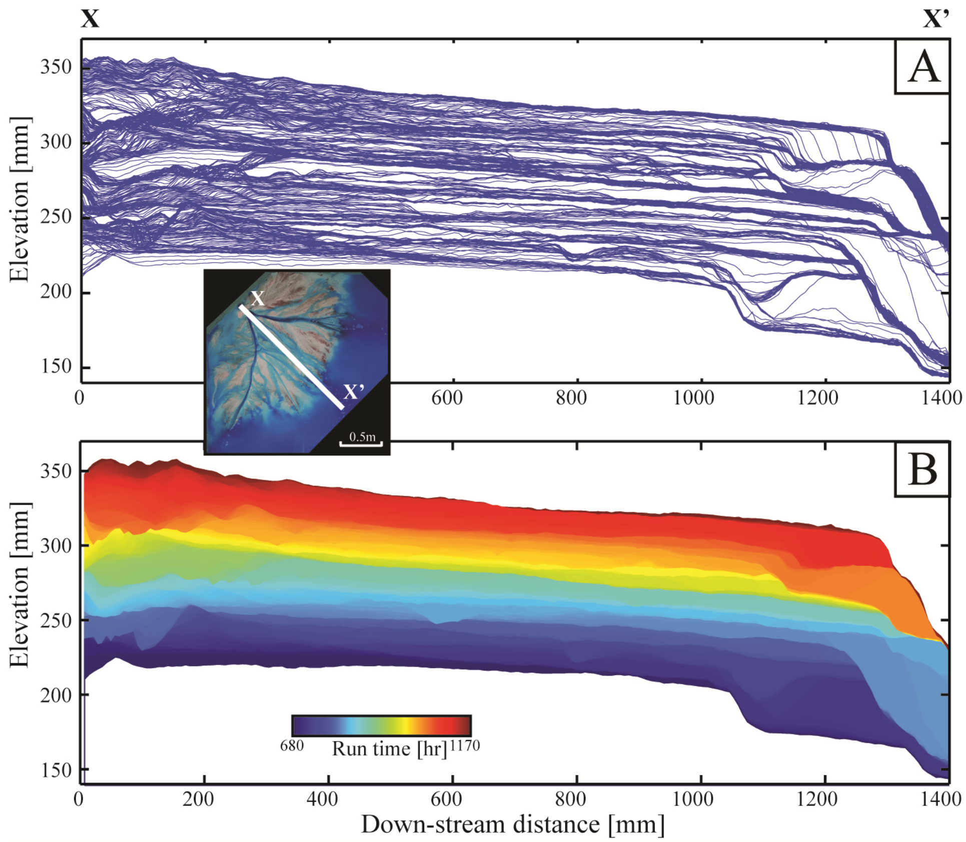

Fig. S5: **Synthetic stratigraphy along a dip transect initiating at the basin entrance and extending 1400 mm in the distal direction (X – X').** A) Synthetic stratigraphy generated from stacked topographic transects clipped for erosion. B) Synthetic stratigraphy with color defining time of sediment deposition.

Fig. S6: **Location map of river deltas used in compilation of field scale systems.** Red dots give locations of deltas used in compilation. Numbers correspond to deltas listed in Table S2.

Movie S1: Overhead time-lapse of control experiment (TDB-12-1). Video shown at 13,500 times actual speed. Tick marks on edge of video occur every 0.5 m.

Movie S2: Overhead time-lapse of $0.5H^*$ $0.5T^*$ experiment (TDB-14-2-S2). Video shown at 13,500 times actual speed. Dye alternates color every $2T_c$ of run-time. Tick marks on edge of video occur every 0.5 m. Long term rise in sea level is de-trended from plot displayed at base of movie.

Movie S3: Overhead time-lapse of $2H^*$ $0.5T^*$ experiment (TDB-15-1-S2). Video shown at 13,500 times actual speed. Dye alternates color every $2T_c$ of run-time. Tick marks on edge of video occur every 0.5 m. Long term rise in sea level is de-trended from plot displayed at base of movie.

Movie S4: Overhead time-lapse of $0.5H^*$ $2T^*$ experiment (TDB-15-1-S1). Video shown at 13,500 times actual speed. Dye alternates color every $2T_c$ of run-time. Tick marks on edge of video occur every 0.5 m. Long term rise in sea level is de-trended from plot displayed at base of movie.

Supplemental References

1 von der Heydt, A., Grossmann, S. & Lohse, D. Response maxima in modulated turbulence. II. Numerical simulations. *Phys Rev E* **68**, doi:Artn 066302

10.1103/Physreve.68.066302 (2003).

2 Jerolmack, D. J. & Paola, C. Shredding of environmental signals by sediment transport. *Geophysical Research Letters* **37**, L19401, doi:10.1029/2010GL044638 (2010).

3 Thomson, D. J. Spectrum estimation and harmonic analysis. *Proceedings of the IEEE* **70**, 1055-1096 (1982).

4 Meyers, S. R. Seeing red in cyclic stratigraphy: Spectral noise estimation for astrochronology. *Paleoceanography* **27**, 12, doi:10.1029/2012PA002307 (2012).

5 Karamitopoulos, P., Weltje, G. J. & Dalman, R. Allogenic controls on autogenic variability in fluvio-deltaic systems: inferences from analysis of synthetic stratigraphy. *Basin Research* **26**, 767-779 (2014).

6 Hoyal, D. C. J. D. & Sheets, B. A. Morphodynamic evolution of experimental cohesive deltas. *Journal of Geophysical Research-Earth Surface* **114**, F02009, doi:10.1029/2007JF000882 (2009).

7 Sadler, P. M. Sediment accumulation rates and the completeness of stratigraphic sections. *Journal of Geology* **89**, 569-584 (1981).

8 Jerolmack, D. J. & Sadler, P. Transience and persistence in the depositional record of continental margins. *Journal of Geophysical Research-Earth Surface* **112**, F03S13, doi:10.1029/2006JF000555 (2007).

9 MacKee, E. D., Nordin, C. F. & Perez-Hernandez, D. Vol. United States Geological Survey water-supply paper ISSN 0083; 2326/A-B (United States Government Printing Office, Washington, D.C., 1998).

10 Allison, M. Historical changes in the Ganges-Brahmaputra delta front. *Journal of Coastal Research*, 1269-1275 (1998).

11 Nittrouer, J. A., Allison, M. A. & Campanella, R. Bedform transport rates for the lowermost Mississippi River. *Journal of Geophysical Research-Earth Surface* **113**, -, doi:Artn F03004

Doi 10.1029/2007jf000795 (2008).

12 Wang, X. & Andutta, F. *Sediment transport dynamics in ports, estuaries and other coastal environments*. 37 (INTECH Open Access Publisher, 2013).

13 Said, R. *The River Nile: Geology, hydrology and utilization*. 320 (Elsevier, 1993).

14 Oomkens, E. Lithofacies relations in the Late Quaternary Niger delta complex. *Sedimentology* **21**, 195-222 (1974).

15 Inam, A. *et al.* The geographic, geological and oceanographic setting of the Indus River. *Large rivers: geomorphology and management*, 333-345 (2007).

16 Sandal, S. T. *The geology and hydrocarbon resources of Negara Brunei Darussalam*. (Brunei Shell Petroleum Company Sendirian Berhad and Brunei Museumm, 1996).

17 Hill, P. R., Lewis, C. P., Desmarais, S., Kauppaymuthoo, V. & Rais, H. The Mackenzie Delta: Sedimentary processes and facies of a high-latitude, fine-grained delta. *Sedimentology* **48**, 1047-1078 (2001).

18 Hijma, M. P., Cohen, K., Hoffmann, G., Van der Spek, A. J. & Stouthamer, E. From river valley to estuary: the evolution of the Rhine mouth in the early to middle Holocene (western Netherlands, Rhine-Meuse delta). *Netherlands journal of geosciences* **88**, 13-53 (2009).

19 Banfield, L. A. & Anderson, J. B. in *Late Quaternary Stratigraphic Evolution of the Northren Gulf of Mexico Margin, SEPM Special Publication No. 79* (eds J.B. Anderson & R.H. Fillon) 289-306 (SEPM (Society for Sedimentary Geology), 2004).

20 Wood, L. J. Chronostratigraphy and tectonostratigraphy of the Columbus Basin, eastern offshore Trinidad. *AAPG Bulletin* **84**, 1905-1928 (2000).

21 Lindsay, J., Holliday, D. W. & Hulbert, A. G. Sequence Stratigraphy and the Evolution of the Ganges-Brahmaputra Delta Complex. *AAPG Bulletin* **75**, 1233-1254 (1991).

22 Straub, K. M., Paola, C., Mohrig, D., Wolinsky, M. A. & George, T. Compensational stacking of channelized sedimentary deposits. *Journal of Sedimentary Research* **79**, 673-688 (2009).

23 Chen, Z. & Stanley, D. J. Quaternary Subsidence and River Channel Migration in the Yangtze Delta Plain, Eastern China. *Journal of Coastal Research* **11**, 927-945 (1995).

24 Abu El-Ella, R. THE NEOGENE-QUATERNARY SECTION IN THE NILE DELTA, EGYPT: GEOLOGY AND HYDROCARBON POTENTIAL. *Journal of Petroleum Geology* **13**, 329-340 (1990).

25 Cui, S. *et al.* Seismic stratigraphy of the quaternary Yellow River delta, Bohai Sea, eastern China. *Marine Geophysical Researchers* **29**, 27-42 (2008).

26 Chukwueke, C., Thomas, G. & Delfaud, J. Processus sédimentaires, eustatisme, subsidence et flux thermique dans la partie distale du Delta du Niger. *Bulletin des Centre de Recherches Exploration-Production Elf-Aquitaine* **16**, 137-186 (1992).

27 Carminati, E. & Martinelli, G. Subsidence rates in the Po Plain, northern Italy: the relative impact of natural and anthropogenic causation. *Engineering Geology* **66**, 241-255 (2002).

28 Clift, P. *et al.* The stratigraphic evolution of the Indus Fan and the history of sedimentation in the Arabian Sea. *Marine Geophysical Researchers* **23**, 223-245 (2002).

29 Saller, A. & Blake, G. in *Tropical deltas of Southeast Asia - Sedimentology, stratigraphy, and petroleum geology: SEPM (Society for Sedimentary Geology) Special Publication 76* (ed F. Hasan Sidi) 219-234 (2003).

30 Wang, Y. & Evans, M. E. Paleomagnetism of Canadian Artic permafrost; Quaternary magnetostratigraphy of the Mackenzi Delta. *Canadian Journal of Earth Sciences* **34**, 135-139 (1997).

31 Zagwijn, W. H. The Netherlands during the Tertiary and Quaternary. A case history of Coastal lowland evolution. *Geologie en Mijnbouw* **68**, 107-120 (1989).